Neural response dynamics of spiking and local field potential activity depend on CRT monitor refresh rate in the tree shrew primary visual cortex

Julia Veit, Anwesha Bhattacharyya, Robert Kretz and Gregor Rainer

J Neurophysiol 106:2303-2313, 2011. First published 17 August 2011; doi:10.1152/jn.00388.2011

You might find this additional info useful...

This article cites 42 articles, 21 of which can be accessed free at:
http://jn.physiology.org/content/106/5/2303.full.html#ref-list-1

Updated information and services including high resolution figures, can be found at:
http://jn.physiology.org/content/106/5/2303.full.html

Additional material and information about ***Journal of Neurophysiology*** can be found at:
http://www.the-aps.org/publications/jn

This infomation is current as of January 24, 2012.

Journal of Neurophysiology publishes original articles on the function of the nervous system. It is published 12 times a year (monthly) by the American Physiological Society, 9650 Rockville Pike, Bethesda MD 20814-3991. Copyright © 2011 by the American Physiological Society. ISSN: 0022-3077, ESSN: 1522-1598. Visit our website at http://www.the-aps.org/.

Downloaded from jn.physiology.org on January 24, 2012

J Neurophysiol 106: 2303–2313, 2011.
First published August 17, 2011; doi:10.1152/jn.00388.2011.

Neural response dynamics of spiking and local field potential activity depend on CRT monitor refresh rate in the tree shrew primary visual cortex

Julia Veit,[1,2] Anwesha Bhattacharyya,[1,2] Robert Kretz,[3] and Gregor Rainer[1,2]
[1]*Visual Cognition Laboratory, Department of Medicine,* [2]*Fribourg Center For Cognition, and* [3]*Division of Anatomy, University of Fribourg, Fribourg, Switzerland*

Submitted 2 May 2011; accepted in final form 11 August 2011

Veit J, Bhattacharyya A, Kretz R, Rainer G. Neural response dynamics of spiking and local field potential activity depend on CRT monitor refresh rate in the tree shrew primary visual cortex. *J Neurophysiol* 106: 2303–2313, 2011. First published August 17, 2011; doi:10.1152/jn.00388.2011.—Entrainment of neural activity to luminance impulses during the refresh of cathode ray tube monitor displays has been observed in the primary visual cortex (V1) of humans and macaque monkeys. This entrainment is of interest because it tends to temporally align and thus synchronize neural responses at the millisecond timescale. Here we show that, in tree shrew V1, both spiking and local field potential activity are also entrained at cathode ray tube refresh rates of 120, 90, and 60 Hz, with weakest but still significant entrainment even at 120 Hz, and strongest entrainment occurring in cortical input layer IV. For both luminance increments ("white" stimuli) and decrements ("black" stimuli), refresh rate had a strong impact on the temporal dynamics of the neural response for subsequent luminance impulses. Whereas there was rapid, strong attenuation of spikes and local field potential to prolonged visual stimuli composed of luminance impulses presented at 120 Hz, attenuation was nearly absent at 60-Hz refresh rate. In addition, neural onset latencies were shortest at 120 Hz and substantially increased, by ~15 ms, at 60 Hz. In terms of neural response amplitude, black responses dominated white responses at all three refresh rates. However, black/white differences were much larger at 60 Hz than at higher refresh rates, suggesting a mechanism that is sensitive to stimulus timing. Taken together, our findings reveal many similarities between V1 of macaque and tree shrew, while underscoring a greater temporal sensitivity of the tree shrew visual system.

electrophysiology; response latency; spike timing; neural coding

TREE SHREWS ARE THE CLOSEST living relatives of primates and diverged from the rest of the Euarchonta clade ~85 million years ago (Liu et al. 2001). They are day-active mammals with a highly developed visual system, comprising at least three distinct retinotopic visual areas in addition to a large primary visual cortex (V1) (Sesma et al. 1984; Wong and Kaas 2009). Tree shrew V1 shares many features with that of primates, such as, for example, orientation columns (Bosking et al. 2002), which are not seen in rodent visual cortex (Van Hooser et al. 2005). Using cathode ray tube (CRT) stimulation delivering precisely timed and predictable luminance impulses lasting ~2 ms, neural responses in macaque V1 have been shown to become aligned to these luminance impulses, particularly for high-contrast visual stimulation (Williams et al. 2004). This entrainment is of interest, because it tends to temporally align visual responses and will thus strongly enhance synchronization of responses among neurons. Here we were interested in examining whether such entrainment to CRT monitor stimulation also occurs in tree shrew V1, and to compare its magnitude and extent with findings in macaques. These issues are relevant for understanding how visual functions in primates evolved from a common ancestor, and for evaluating the similarity of tree shrew and macaque V1 in terms of temporal neural response dynamics. We found that both spiking and local field potential (LFP) activity were strongly entrained to CRT monitor refresh rate, and that entrainment decreased with increasing CRT refresh rate.

During CRT monitor stimulation, each luminance impulse can be regarded as a separate, briefly flashed stimulus. By varying the refresh rate, we could thus deliver luminance impulses separated by different time intervals. Here, we used three refresh rates to investigate how changes in the temporal stimulus profile during a stimulation period of ~80 ms affect cortical responses. Higher refresh rates are usually preferred, because they more closely approximate the continuous nature of the visual environment. We found that, at 120-Hz refresh rate, the neural response declined rapidly during the 80-ms stimulus presentation period, such that each successive luminance impulse evoked progressively less activity. At 60 Hz, however, responses to subsequent luminance impulses were nearly independent of each other and decreased little over the course of stimulus presentation. Finally, we examined temporal dynamics of neural responses separately for visual stimuli with luminance increments (white) and decrements (black) relative to the background. We found dominance for black stimuli in terms of latency and response magnitude, which was most striking at low refresh rates.

MATERIAL AND METHODS

Animal preparation. Experiments were performed on six adult tree shrews (*Tupaia belangeri*), aged 2–5 yr. Animals initially received ketanarkon (im, 100 mg/kg) and atropine (im, 0.02 mg/kg). We then performed a tracheotomy and administered the muscle relaxant pancuronium bromide (ip, initial dose 0.4 mg/kg, then 0.2 mg/kg approximately every 45 min). Animals were artificially respirated at 100 strokes/min (Harvard Instruments Respirator) using a mixture of 70% N_2O and 30% oxycarbon (95% O_2/5% CO_2) and isoflurane (0.5–1.5%). Animals were then transferred to a stereotaxic device (David Kopf) that was modified to permit visual stimulation. Animals wore contact lenses to prevent drying of eyes. An eye drop of atropine was applied to the eye for pupil dilation. Visual stimulation was monocular; the other eye was covered. To gain access to V1, the temporal muscle was removed, the bone cleaned, and a hole (~2–3 mm diameter) was drilled around anteroposterior −1 mm and mediolateral +4 mm. A small slit was made in the dura using a syringe needle to permit introduction of the tetrodes into the cortex. After tetrode

Address for reprint requests and other correspondence: G. Rainer, Visual Cognition Laboratory, Dept. of Medicine, Univ. of Fribourg, Chemin du Musée 5, CH-1700 Fribourg, Switzerland (e-mail: gregor.rainer@unifr.ch).

0022-3077/11 Copyright © 2011 the American Physiological Society

Downloaded from jn.physiology.org on January 24, 2012

placement, the cortex was covered with handwarm 2% agarose (in 0.9% NaCl) to prevent drying and provide stability. During the entire experiment, body temperature was maintained at 37°C via an electric heating pad controlled by a rectal thermal probe. Heart rate was monitored using a Tektronix differential amplifier, with typical values ranging from 380 to 420 beats/min. All procedures were conducted according to local regulation approved by the veterinary office of the Canton of Fribourg.

Electrophysiology. Tetrodes were fabricated by twisting together four 12.5-μm-diameter nickel-chromium wires (RO-800; Kanthal Precision Technology), and the impedances were reduced to 200–300 kΩ by gold plating. Two tetrodes spaced ~300 μm apart were advanced into V1 using a hydraulic microdrive (David Kopf Instruments). Identical penetrations were made in all experiments normal to the cortical surface in a saggital plane, by tilting the microdrive backwards at an angle of 30°. Since we did not tilt the electrode laterally, an angle of 25° remained between the penetration path and the surface normal vector (see the projection of the penetration path onto a coronal section and the surface normal vector in Fig. 1*A*). The cortical depth of the recorded units was computed by correcting the penetration depth using an appropriate factor [cos (25°) = 0.92]. For a given penetration, we recorded activity at multiple depths typically spaced around 200 μm apart. The signal was amplified by a RA16PA Medusa preamplifier and then filtered and digitized by a RZ5 Bioamp Processor (Tucker-Davis Technologies, Alachua, FL). LFPs were filtered between 1 and 200 Hz and sampled at 509 Hz. Spike waveforms were recorded by thresholding the signal filtered between 300 Hz and 4 kHz and sampled at 24.4 kHz. The spike waveforms were sorted into clusters corresponding to single neurons using the public domain software MClust 3.5 where possible. In total, we identified single neurons at 26 sites and multiunit activity at 26 additional sites. Since we observed no functional differences between single and multineuron activity, these were grouped together for all analyses.

Histology. At the end of a recording session, electrolytic lesions were made at multiple sites using a constant-current stimulator (WPI A360) passing 10 μA for 10 s. Animals were perfused with 0.9% NaCl followed by ice-cold 4% paraformaldehyde in 0.1 M phosphate buffer (pH 7.4). The top of the skull was removed, and a coronal cut was made through the brain at anteroposterior +4 mm in the stereotaxic frame. The brain was then removed and immersed in a mixture of 2% DMSO and first 10% and later 20% glycerol in 0.1 M phosphate buffer (pH 7.4). The posterior part of the brain was then cut into 50-μm sections using a freezing microtome (Microm HM440E). The lesions were located in Nissl-stained coronal sections. Because our track was not in a coronal plane, the lesions were on different

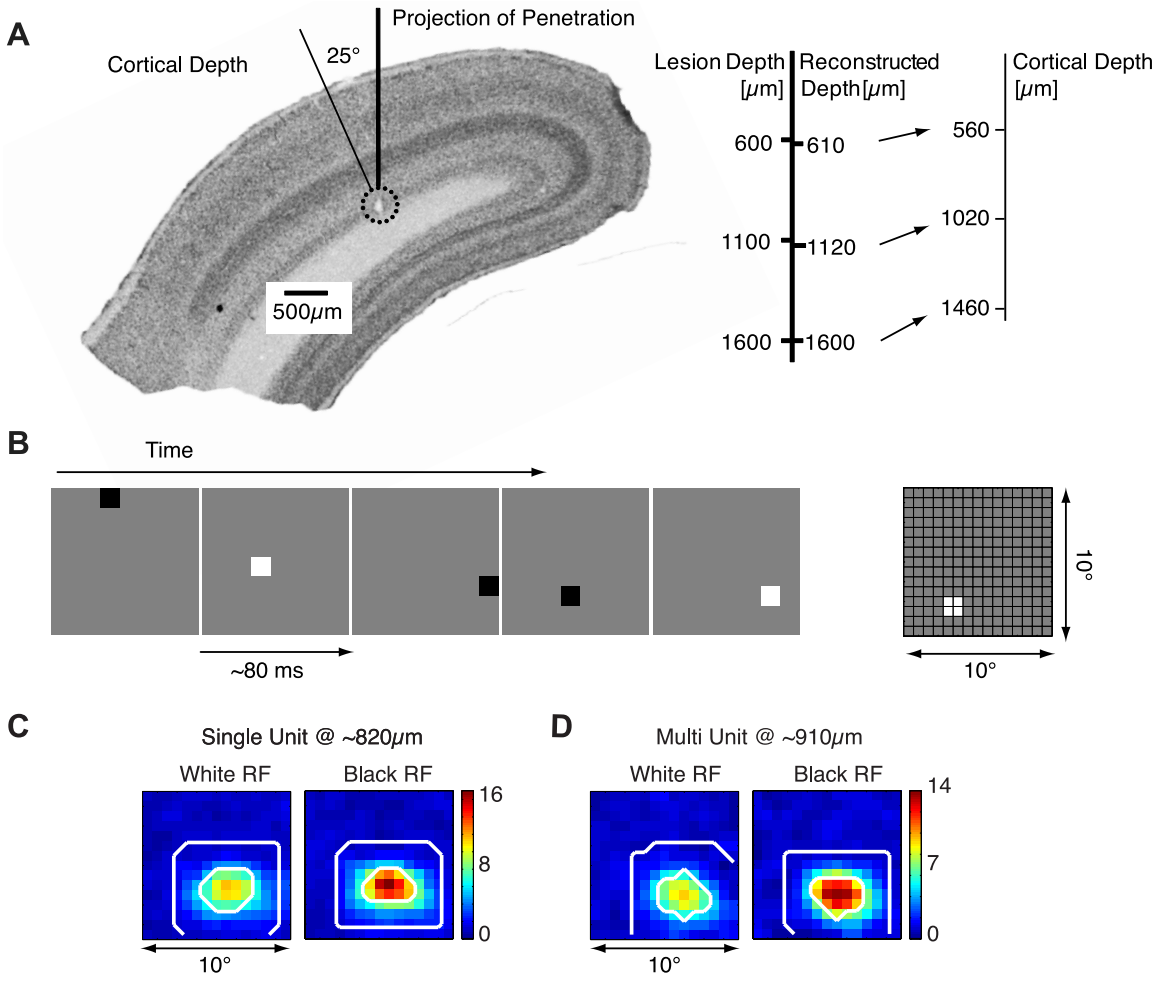

Fig. 1. Depth reconstruction and paradigm. *A*: projection of an electrode track is shown onto a 50-μm-thick Nissl-stained coronal section of the primary visual cortex, with layer IV clearly visible in dark staining. One electrolytic lesion, marked by the dotted circle, is visible in this section. *B*: sparse noise consists of dark or bright squares presented in pseudorandom order on a 15 × 15 position rectangular grid spanning 10 × 10 visual degrees over an intermediate luminance background shown for ~80 ms, with no interstimulus time. *C*: receptive fields (RF) for white and black stimuli are shown in the *left* and *right* panels, respectively, for an example single unit. The inner white lines determine the area that is considered to be within the RF. Every trial that showed a stimulus outside the outer white line was considered a background trial, as there was only gray inside the RF and its immediate surround. *D*: same as *C* for an example multiunit from the same animal, but at a different recording location.

Downloaded from jn.physiology.org on January 24, 2012

sections. If a lesion was visible in more than one adjacent section, we chose the section with the relatively largest lesion as the reconstructed depth of the lesion. The cortical depth of each recording site was reconstructed relative to a reference lesion at the deepest recording site, accounting for brain shrinkage due to histological processing of around 8–17%.

Stimuli. Stimuli were generated with Psychophysics Toolbox running on a Mac Mini and presented on a gamma corrected 21-in. diameter (~56.7° visual angle) Compaq Qvision 210 CRT monitor running at either 119.22 (120 Hz), 89.73 (90 Hz), or 60.31 Hz (60 Hz). A single luminance impulse decayed with a time constant of ~2 ms, as measured with a light-sensitive diode and an oscilloscope. Maximum luminance measured with a Minolta TV-color analyzer was determined as 50 cd/m^2 and "white", "gray", and "black" values were adjusted to have 100, 50, and 0% of this value, respectively. Before recording, we mapped the approximate location of the receptive field of the unit under study by manually sliding bars generated with a simple graphics program back and forth on the monitor. The stimulus was then positioned in this area at eccentricities between 7° and 17°. We employed the sparse noise stimulus, consisting of a sequence of randomly positioned white and black squares over a gray background. In most cases, 1.3 × 1.3° black or white squares were positioned on a 15 × 15 grid with 50% overlap between adjacent positions, spanning a total area of 10 × 10°. To avoid edge effects and to obtain a homogenously sampled surface with the overlapping stimuli, we actually showed 16 × 16 pixel positions spanning 11.3 visual degrees and removed a 0.5-pixel-wide border from each side after weighting of the pixels. Each black or white square was presented for a total duration of ~80 ms (83.3 ms at 120 and 60 Hz, 77.7 ms at 90 Hz), corresponding to 10, 7, and 5 video frames at refresh rates of 120, 90, and 60 Hz, respectively. There was no blank period between subsequent stimuli. The sequence of all stimuli was repeated 10 times in different pseudorandom orders. Altogether, the sequence usually lasted for ~7 min {total of 512 stimuli [16 × 16 pixel positions × 2 (black and white)], each shown 10 times for ~80 ms}.

We also employed a white noise stimulus at every location and for all refresh rates. The spatial extent was the same as for the sparse noise stimulus at each location, but all pixel positions were filled randomly with 50% white and 50% black squares. Note that the pixel size during white noise stimulation was one-half the width and height of a sparse noise pixel that always filled two adjacent pixel positions. We generated 2,000 individual random stimuli, and each stimulus was presented for the same time as the sparse noise: 10 frames at 120 Hz, 7 frames at 90 Hz, 5 frames at 60 Hz. The entire sequence lasted ~3 min for white noise (2,000 stimuli, each shown for ~80 ms).

Locking ratio. We calculated the locking ratio (LR) as the ratio of the mean Fourier components at the refresh rate to the mean Fourier components of the surrounding 20 Hz (Williams et al. 2004).

$$LR = \frac{\frac{1}{N}\sum_i |z_i|^2}{\frac{1}{M}\sum_i |y_i|^2}$$

where the z_i are N independent estimates of the Fourier components at the refresh rate (120, 90, or 60 Hz), and the y_i are M independent estimates of the Fourier components in the 20 Hz surrounding the frame rate (110–130, 80–100, or 50–70 Hz). LFPs were upsampled to 1 kHz, and spike trains binned into 1-ms bins to yield signals with equal temporal resolution. Both signals were cut into usually $N = 26$ (120 and 60 Hz) or $N = 24$ (90 Hz) non-overlapping snippets of ~16.4 s. Fourier components were estimated for each snippet using a rectangular window without tapering. For the power estimates of the surrounding frequencies, the component at the frame rate, as well as 1.8 Hz to either side, were excluded. Thus 269 estimates of power at the surrounding frequencies were gathered for each snippet of data. To determine whether a unit was significantly entrained to the frame rate of the monitor, we bootstrapped a distribution from these power values of the surrounding frequencies and recalculated the locking ratio exactly as described above. We repeated this procedure 1,000 times and took the upper 1% value as threshold for significance. For the analyses shown in Fig. 3, a running average of the locking ratio across nine neighboring recording depths was normalized to lie between values of 0 (minimal locking) and 1 (maximal locking). Normalization was performed separately for the three refresh rates.

Receptive field mapping. Receptive fields were estimated for each unit by weighting each square on the grid with the average number of spikes fired in response to its onset in a window from 25 ms to 110 ms after stimulus onset. Receptive fields were calculated separately for trials with black stimuli and white stimuli. Every square for which the response exceeded a threshold of two standard deviations above the mean firing rate for all trials was considered to be within the receptive field. All units had well-delimited receptive fields in the 120- and 90-Hz conditions. At 60 Hz, receptive fields could not be estimated for white stimuli for nine units and for black stimuli for one unit due to weak responses in this condition. These units were excluded for the latency and amplitude measurements.

Evoked responses. For the peristimulus time histograms (PSTH) and visual evoked potentials (VEP), we averaged spiking activity and LFPs, respectively, of trials where a black or white stimulus was present inside the defined receptive field. We then subtracted the average response to trials, where the stimulus was far (at least three pixel positions distance) from the receptive field. In these trials, only gray background was shown in the area of the receptive field. By subtracting this background-related component, we approximate the pure stimulus-related part of the response (exceeding the response to the background). Because we had no interstimulus interval, there was the possibility of obscuring the "baseline" of the next trial by the still ongoing response to the preceding stimulus. To address this in our analysis, we only consider trials that were preceded by an "outside" trial for both "stimulus inside" and "stimulus outside" averages.

Slopes. To estimate the slope of the attenuation of the responses, we determined the overall peak of the PSTH, for both black and white stimuli, after the PSTH of the background response was subtracted. We then identified all subsequent peaks (usually 7 for 120-Hz, 5 for 90-Hz, and 4 for 60-Hz responses). Peaks were expected to occur for every screen refresh in temporal offsets corresponding to the frame rate. If no clear peak was present around the expected time, as was often the case for the later peaks at 120 Hz, we took the value of the PSTH at the expected time. Linear fits were made through the first five peaks at 120 Hz and all peaks at 90 and 60 Hz. The later peaks at 120 Hz had values close to zero and would have confounded the true attenuation slope. They were thus excluded from the linear fits. The slope for the decline of the VEP was estimated in exactly the same manner, except that in this case the peaks were negative.

Background response. To estimate the magnitude of the response to the redraw of the gray background, we calculated the modulation ratio of the PSTH for trials with only the gray background present in the receptive field. To this end, we identified the peaks in the background PSTH in the same way as described above for the attenuation slope analysis. We then windowed the signal, centered around each peak, resulting in signal snippets with lengths depending on the refresh rate: 8 ms for 120 Hz, 11 ms for 90 Hz, and 17 ms for 60 Hz. These peak snippets were averaged, and the modulation amplitude was determined as the difference between the maximum and the minimum of this mean background redraw evoked peak. We divided this value by the mean firing rate across the gray trials to obtain the modulation ratio. The modulation ratio for the LFPs was calculated in the exact same manner, by averaging the negative peaks and dividing their modulation amplitude by the mean amplitude of the LFP across the gray trials.

Latencies. To estimate onset latency of spiking and LFP activity, we report the time point at which stimulus-evoked activity (back-

Downloaded from jn.physiology.org on January 24, 2012

ground response subtracted) first surpassed four standard deviations of the mean background response. If this threshold was already exceeded by the unit in the period before the visual delay (24 ms), or if it never surpassed this threshold, the unit was excluded due to bad signal-to-noise ratio. At 60 Hz, latencies could frequently not be estimated for white stimuli due to weak responses in this condition.

White-to-black ratio. We calculated the white-to-black ratio similar to Yeh et al (2009) as log (FR_{white}/FR_{black}), the logarithmic ratio of the mean firing rates for "white" compared with "black" stimulus trials. This ratio is zero for equal firing rates and the more negative it is, the more the "black" response dominates the "white".

RESULTS

We present here data collected from V1 in six tree shrews during terminal experiments under isoflurane anesthesia. We recorded single unit, multiunit, and LFP activity from a total of 52 sites, covering all six cortical layers. We confirmed the location of recording sites using electrolytic lesions at reference depths along the recording track using histological analysis (see Fig. 1*A*). We describe robust entrainment of neural responses to the refresh rate of the CRT monitor used for visual stimulation and demonstrate differences in neural activity for different refresh rates, as well as for stimulus luminance increments ("white") and decrements ("black") relative to the intermediate luminance background. We used a sparse noise protocol for visual stimulation, where single spots of light are presented on a 15 × 15 grid, which is positioned over an area that includes the receptive field of the unit under study (see Fig. 1*B*). Receptive fields were similar in size for white and black stimuli, as shown for a single neuron and a multiunit site in Fig. 1, *C* and *D*, respectively. Stimuli were presented in pseudorandom order as a continuous sequence, without intervening blank periods, lasting ~7 min, and each single light spot was presented during a period of ~80 ms, corresponding to 10, 7, and 5 CRT frames for 120-, 90-, and 60-Hz refresh rate, respectively.

Entrainment of spiking and LFP responses to monitor refresh rate. The luminance profile for a CRT monitor pixel is shown in Fig. 2*A* for the three refresh rates we employed in our study (120, 90, 60 Hz). Luminance peaks correspond to the time point of excitation by the cathode ray. The screen refresh time, i.e., the time between peaks, varies with the refresh rate, and pixel luminance decays rapidly with a time constant of ~2 ms, according to our measurements. As seen in Fig. 2*B* for an example neuron, spikes occur in clusters separated by the screen refresh time, and this effect appears most prominent at low refresh rates. Note that spikes appearing at a given time are not actually related to the immediately preceding screen refresh, but are caused by a screen refresh that is ~30 ms in the past. This temporal shift is due to the neuronal response latency, resulting from signal transduction in the retina and action potential transmission to V1. The monitor refresh rate also exerted a strong influence on the LFP signal. In Fig. 2*C*, we show a set of single-trial LFP responses collected at the same cortical site. At 60 Hz, we observe large negative peaks in the LFP occurring at ~17-ms intervals, corresponding to the time between screen refreshes. These peaks are thus evidence of robust entrainment. At 90- and 120-Hz monitor refresh rates, entrainment corresponds to LFP peaks separated by 11 and 8 ms, respectively. As can be seen in Fig. 2*C*, LFP entrainment appears to decrease with increasing monitor refresh rate.

To quantify the entrainment of spike and LFP signals, we used an established method based on Fourier decomposition (Williams et al. 2004). Briefly, we determined a locking ratio by dividing the Fourier component at the monitor refresh rate by the average Fourier components of the surrounding frequencies. The average LRs for LFP (mean ± SE: LR_{120}: 6.6 ± 0.5, LR_{90}: 18.1 ± 1.1, LR_{60}: 21.6 ± 1.4) and spikes (mean ± SE:

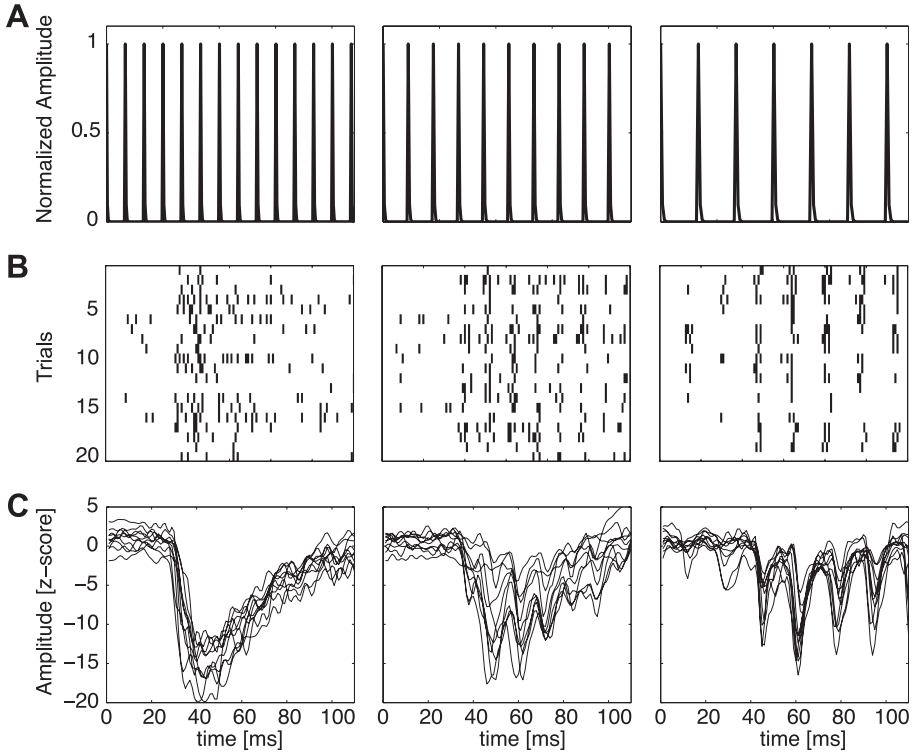

Fig. 2. Entrainment of neural responses to cathode ray tube (CRT) monitor refresh. *A*: luminance profile of the CRT monitor at the three examined refresh rates. Brief luminance peaks occur every 8.3, 11.1, and 16.6 ms for refresh rates of 120, 90, and 60 Hz, respectively. *B*: raster plot of 20 trials of spikes recorded from one example primary visual cortex (V1) neuron in response to sparse-noise stimulation at the various refresh rates. Every line corresponds to one trial, and every tick to one spike. *C*: 10 single-trial local field potential (LFP) amplitude traces from the same recording site.

Downloaded from jn.physiology.org on January 24, 2012

LR_{120}: 2.7 ± 0.2, LR_{90}: 6.2 ± 0.5, LR_{60}: 10.2 ± 1.3) are shown in Fig. 3*A*. These quantitative analyses show that entrainment was dependent on the monitor refresh rate (one-way ANOVA: LFPs: $P < 0.001$, spikes $P < 0.001$). Using a bootstrap analysis (see MATERIALS AND METHODS), we estimate that neural signals recorded at all ($n = 52$) of our sites were significantly entrained to all stimulus frequencies (bootstrapping method, $P < 0.01$). Entrainment was strongest at 60 Hz and declined with increasing monitor refresh rate for both signals. At 120 Hz, we observed weaker but still significant entrainment in both signals. LRs for spikes and LFPs recorded at the same cortical site were strongly correlated [120 Hz: *R* value, 0.65 ($P < 0.001$), 90 Hz: *R* value: 0.50 ($P < 0.001$), 60 Hz: *R* value: 0.65 ($P < 0.001$)]. Thus sites with strong LFP entrainment also showed strong entrainment of spikes to the monitor refresh rate.

Previous studies (Williams et al. 2004) found the magnitude of the entrainment to be dependent on the stimulus contrast. To address this issue, we recorded neural activity for each site also during the presentation of white noise, where each grid location contains either a white or black stimulus varying randomly in time. This stimulus thus has similar overall luminance compared with sparse noise, but higher contrast. We observed two- to threefold increases in locking ratio for white noise compared with sparse noise stimuli, which was significant across all refresh rates for both spikes and LFPs (paired *t*-tests: $P \ll 0.001$), indicating that entrainment to the CRT refresh rate is contrast dependent. Note that LRs are computed based on the continuous time series of recorded data, thus including stimulation conditions both inside and outside the receptive field as well as white and black stimuli, and are thus not directly comparable to the trial-averaged neural data presented further below.

We examined entrainment of spiking and LFP activity as a function of the depth at which neural activity was recorded. As in previous studies in macaque monkey (Williams et al. 2004), we found that locking tended to be strongest in intermediate layers of the visual cortex, at depths between 700 and 1,000 μm. For example, LRs obtained for spiking activity at a monitor refresh rate of 90 Hz are shown in Fig. 3*B* as a function of recording depth. Recording locations with strong LRs are shaded in black and were found exclusively at cortical depths between ~700 and 1,000 μm. This depth corresponds to the granular input layer IV of the visual cortex, where signals arrive from the lateral geniculate nucleus. We computed the mean normalized locking ratio as a function of recording depth for spiking activity at the three monitor refresh rates. As shown in Fig. 3*C*, locking was generally strongest for layer IV units, whereas locking was weakest for supragranular layer units. Interestingly, locking for infragranular units appeared to depend on monitor refresh rate, such that it was relatively weak for 90 and 120 Hz, but elevated for 60 Hz. Since the deep layers communicate with subcortical areas, this enhanced entrainment may result from a frequency-dependent interaction with other prominent visual structures, such as the superior colliculus or pulvinar (Grieve et al. 2000; Shipp 2004). The variation of LRs with recording depth for the LFP is shown in Fig. 3*D*. As for spiking activity, LFP LRs were highest in layer IV, regardless of monitor refresh rate. These results reveal substantial differences between the cortical layers in terms of temporal locking to the sensory stimulus.

Effect of background redraw on neural activity. Given the strong effects of monitor refresh rate on timing of spiking and LFP responses, we wanted to examine what impact it had on stimulus-evoked neural activity. We noticed that many units showed an entrained response when the black or white stimulus was presented at a location outside the receptive field, and only

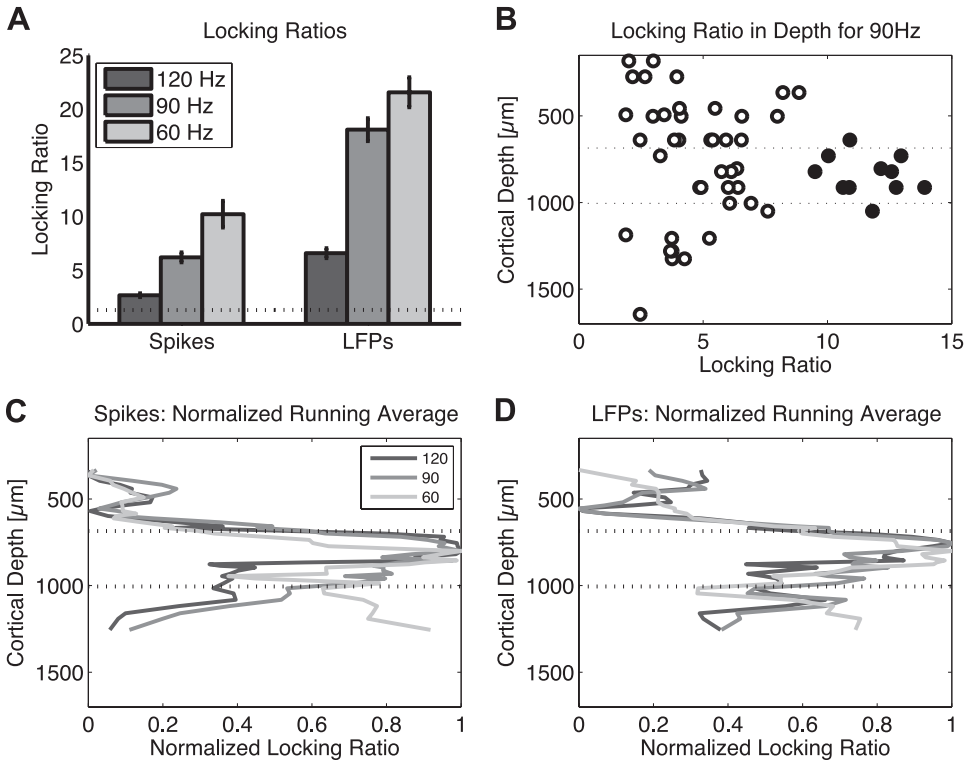

Fig. 3. Quantitative analysis of entrainment to monitor refresh. *A*: bar plots of the mean locking ratio of spiking and LFP activity at the 52 recorded sites at the 3 different refresh rates. The dotted line signifies the 99% significance level, as determined by a bootstrapping method. Error bars: SE. *B*: the locking ratios of individual units plotted against cortical depth for the 90-Hz refresh rate. Units with locking ratios exceeding a criterion value of $\eta = 9$ are solid black. The dotted lines represent the approximate borders of layer IV. *C*: the normalized running averages (of 9 neighboring units) of the locking ratios of spiking activity are plotted against cortical depth for the three refresh rates. The dotted lines represent the approximate borders of layer IV. *D*: same as *C* for LFP activity.

Downloaded from jn.physiology.org on January 24, 2012

the gray background was present inside the receptive field. This "background response" occurred in response to luminance transients associated with the redrawing of the intermediate luminance gray background. In Fig. 4*A*, we show the PSTHs for this background response for an example single unit at the three different refresh rates. It is clearly visible that at 60 Hz the unit responded to every single refresh of the background, whereas at 120 Hz this background response is virtually absent. The example unit had the following average "background modulation ratio" (BMR; modulation amplitude/mean firing rate): BMR_{120}, 0.60; BMR_{90}, 3.06; BMR_{60}, 5.49. Across the population, we observed a similar pattern (mean ± SE; BMR_{120}: 1.0 ± 0.11, BMR_{90}: 2.2 ± 0.13, BMR_{60}: 3.5 ± 0.24), and this effect was significant (one-way ANOVA: $P \ll 0.001$).

The LFPs showed the same trend (data not shown) (mean ± SE: BMR_{120}: 0.14 ± 0.010, BMR_{90}: 0.82 ± 0.041, BMR_{60}: 1.39 ± 0.057). A one-way ANOVA showed this difference was significant ($P \ll 0.001$). These findings suggest that the redraw of the gray background is robustly reflected in V1 activity at 60-Hz, but not at 120-Hz refresh rate. Figure 4*B* shows a PSTH of the same single unit over all trials where a black or white dot was presented in the receptive field. At times preceding the visual response delay, the background response from the previous trial is clearly visible. For the majority of the remaining analyses, except where noted, we subtract the trial-averaged background response from the PSTH and VEP (see MATERIALS AND METHODS) as an approximation of the pure stimulus-evoked activity for both spiking and LFP. We note that the background subtraction does not affect the significance of any of the reported results, which are valid similarly for the original data without background activity subtracted. The results for the same example recording site described above are shown in Fig. 5 for white and black stimuli separately. As can be seen, little neural activity is visible at times preceding the visual response latency of ~25 ms, because of the subtraction of the background response. There are, however, some small-amplitude fluctuations, for example at 60-Hz refresh rate, which are remnants of the background activity that were not completely removed by the subtraction procedure. Below, we continue to analyze the temporal dynamics of this evoked activity.

Monitor refresh rate-dependent response dynamics of neural activity. We observed striking differences in neural response dynamics for the different monitor refresh rates. The PSTH of an example single unit, shown in Fig. 5*A*, reveals that spikes were indeed strongly entrained to the screen refresh, particularly at 60 and 90 Hz, consistent with the above quantitative analyses. Entrainment occurred for both white and black stimuli. At 60 Hz, individual CRT luminance impulses elicited neural responses that were almost completely separable from each other in time. By contrast, at 120 Hz, there was considerable overlap between neural activation peaks elicited by subsequent screen refreshes. Interestingly, these overlapping peaks add up in a highly nonlinear fashion: responses to subsequent screen refreshes at 120 Hz are strongly attenuated, unlike in the 60-Hz condition, where every frame elicits responses of approximately equal magnitude. To quantify this response attenuation, we computed the slope m of a fit through the individual response peaks in a time window from ~50 to 110 ms following stimulus onset. For the example neuron from Fig. 5*A*, we obtained the following values: $m_{120,white} = -2.9$, $m_{120,black} = -7.4$, $m_{90,white} = -3.0$, $m_{90,black} = -5.2$, $m_{60,white} = -0.1$, and $m_{60,black} = -1.7$ Hz/ms. These values were similar to the average values across all recorded units, shown in Fig. 6*A*. A two-way ANOVA using white/black and refresh rates as factors revealed significant effects of refresh rate ($P \ll 0.001$) and of black/white ($p < 0.01$) on neuronal response attenuation.

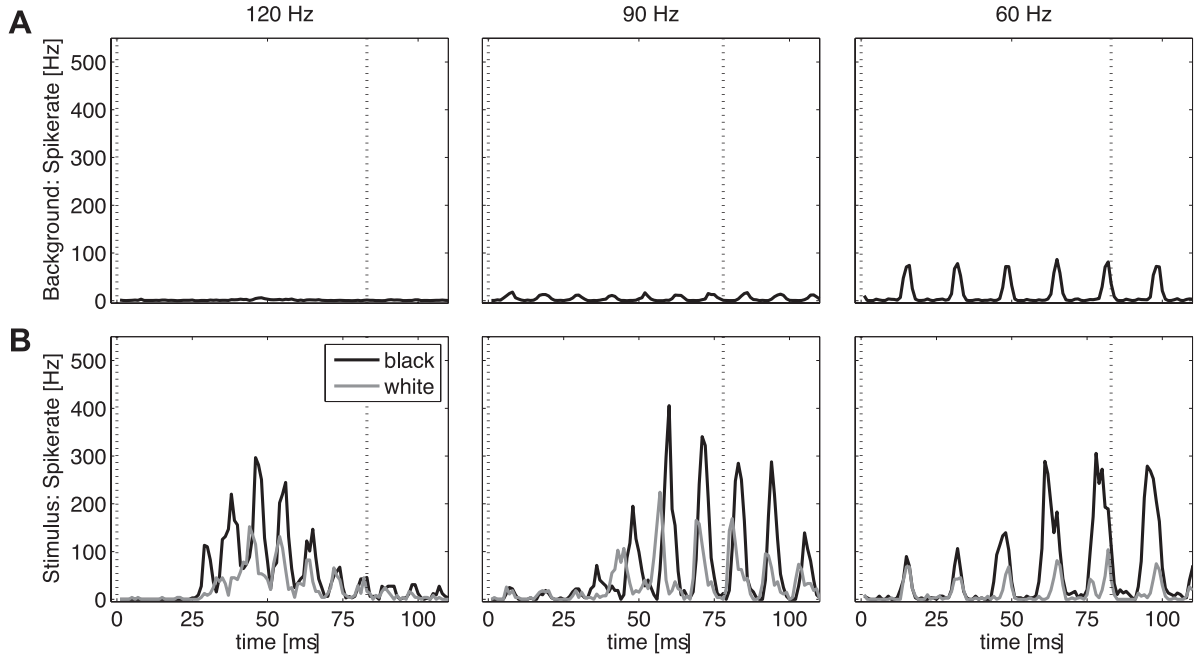

Fig. 4. Effects of CRT refresh rate on neural responses. *A*: average spiking responses of one example neuron to trials showing only gray background in the RF at all refresh rates. Dotted lines represent stimulus on- and offset. *B*: average spiking responses of the same example neuron to "black" stimuli (black traces) and "white" sparse noise stimuli (gray traces) shown in the RF. Dotted lines represent stimulus on- and offset.

Downloaded from jn.physiology.org on January 24, 2012

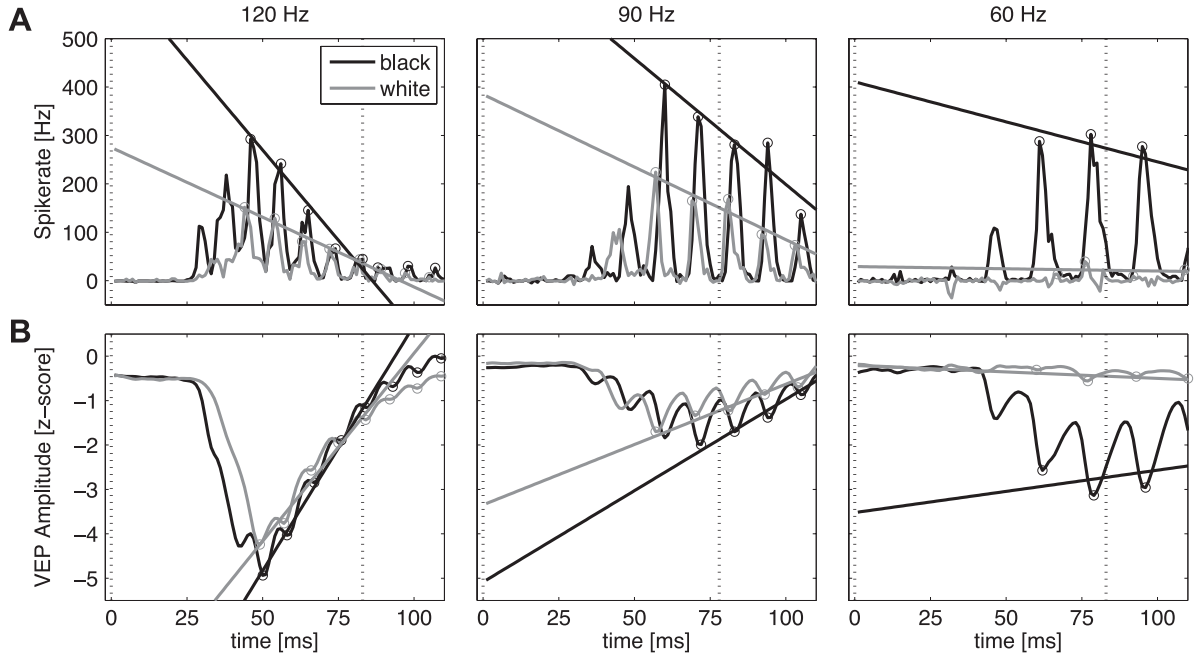

Fig. 5. Effects of CRT refresh rate on time course and attenuation of stimulus-related neural responses. *A*: average spiking response time courses of one example neuron at 1-ms resolution plotted separately for black stimuli (black traces) and white stimuli (gray traces), with the average background response subtracted to approximate pure stimulus-related activity. The thick black and gray bars are linear fits through the response peaks to determine the slope of the decline of neural activity as a measure of attenuation. Dotted lines represent stimulus on- and offset. *B*: same as *A* for trial-averaged LFP activity at the same cortical location as *A*. VEP, visual evoked potential.

The above analyses indicate that neural activity remained relatively constant for subsequent screen refreshes at 60 Hz, but declined rapidly at higher refresh rates. Indeed, at the end of the visual response period around 110 ms after stimulus onset, only a fraction of the maximum response to the luminance impulse at the beginning of the visual stimulation period remained (response remaining: $RR_{120,white} = 5\%$, $RR_{120,black} = 9\%$, $RR_{90,white} = 16\%$, $RR_{90,black} = 34\%$, $RR_{60,white} = 55\%$, and $RR_{60,black} = 67\%$) compared with the activity of the highest peak for the example neuron (Fig. 5*A*). These values were similar to the average values across all recorded units, shown in Fig. 6*B*. According to a two-way ANOVA using white/black and refresh rate as factors, the effect of refresh rate was significant ($P \ll 0.001$), but there was no main effect of black/white ($P > 0.1$). Together, these findings suggest that there was minimal neural response decline at 60-Hz refresh rate, indicative of near independence of neural responses to subsequent screen refreshes. On the contrary, the

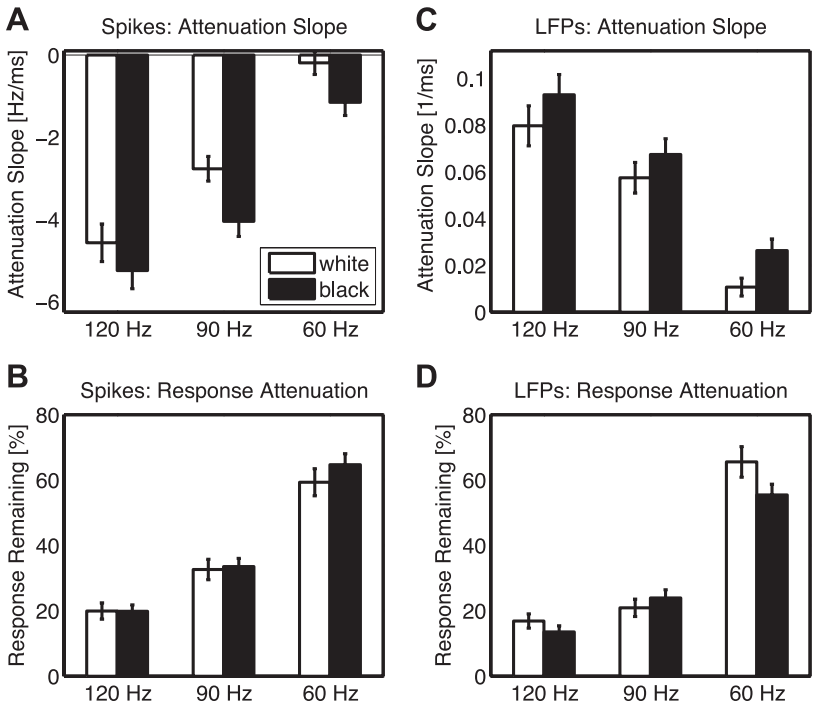

Fig. 6. Attenuation: population analysis. *A*: average values for the slope of a linear fit through the individual peaks of the peristimulus time histograms (PSTH) for each of the 52 recorded units, separately for black (black bars) and white (white bars) responses at all refresh rates. Error bars: SE. *B*: ratio of the value for a peak at the end of the response (around 110 ms) to the value of the peak at the maximum of the response (around 40 ms). Low values indicate high attenuation, because the response declines to repeated frames of the stimulus. High values indicate near independence of the peaks evoked by repeated monitor refreshes. Error bars: SE. *C*: same as *A* for a fit through the peaks of the VEP. *D*: same as *B* for the LFP.

Downloaded from jn.physiology.org on January 24, 2012

strong decline observed at 90 and 120 Hz suggests a strong nonlinear dependence among neural responses to luminance impulses generated by subsequent screen refreshes.

Given these strong effects of refresh rate on temporal dynamics of spiking responses, we proceeded to examine whether a similar effect was visible in LFP signals. We found that this was indeed the case: LFP signals from the same cortical site as the spiking activity analyzed above are shown in Fig. 5*B* as a function of monitor refresh rate. Similar to what we observed for spiking activity, there was relatively little overlap between LFP activations elicited by subsequent screen refreshes at 60 Hz, where each refresh elicits a clearly separate signal peak. At 120 Hz, peaks are not clearly discernible, but merged together into a single, nearly continuous response. We quantified refresh rate-dependent LFP attenuation by computing the attenuation slope m in a time window from ~50 to 110 ms following stimulus onset, similar to our analysis of spiking attenuation above. Note that attenuation in LFP signals is associated with positive values of the parameter m. For the recording site in Fig. 5*B*, we obtained the following values: $m_{120,\text{white}} = 0.085$, $m_{120,\text{black}} = 0.111$, $m_{90,\text{white}} = 0.027$, $m_{90,\text{black}} = 0.041$, $m_{60,\text{white}} = -0.003$, $m_{60,\text{black}} = 0.010$ 1/ms. These values were similar to the average values across all LFP sites, as shown in Fig. 6*C*. A two-way ANOVA using white/black and refresh rates as factors revealed a significant effect of both refresh rate ($P \ll 0.001$) and black/white ($P = 0.02$). At the end of the visual response period around 110 ms after stimulus onset, the remaining response to a single screen refresh was $RR_{120,\text{white}} = 11\%$, $RR_{120,\text{black}} = 1\%$, $RR_{90,\text{white}} = 8\%$, $RR_{90,\text{black}} = 7\%$, $RR_{60,\text{white}} = 89\%$, $RR_{60,\text{black}} = 67\%$ compared with the activity to the initial peak activity for the example LFP site (Fig. 5*B*). These values were similar to the average values across all LFP sites, as shown in Fig. 6*D*. According to a two-way ANOVA using white/black and refresh rate as factors, the effect of refresh rate was significant ($P \ll 0.001$), but there was no main effect of black/white ($P > 0.1$).

Effect of monitor refresh rate on average response magnitude and latency. In addition to the effects on temporal dynamics, we also found that CRT refresh rate had a large impact on firing rate and visual response latency. The mean firing rate, analyzed without background response subtraction, during the visual response period (25–110 ms after stimulus onset) averaged across all recorded units, is shown in Fig. 7*A*, as a function of refresh rate and black/white. The magnitude of the mean background response is shown in gray bars as a function of refresh rate for comparison. Since mean firing rate is positively correlated with refresh rate, V1 acts like a high-pass filter for sparse noise stimuli as a function of refresh rate. Interestingly, the opposite is true for activity during stimulation with the uniform gray background. Here, the mean firing rate significantly decreases with increasing refresh rate (one-way ANOVAs, $P < 0.01$), consistent with a low-pass filtering property of V1 in this case. A two-way ANOVA revealed significant effects of both refresh rate and black/white ($P \ll 0.001$) on mean firing rate, with white stimuli evoking less activity than black stimuli. These reductions in activity for white compared with black stimuli were most pronounced at 60 Hz (R_{120}: 29%, R_{90}: 26%, R_{60}: 60%).

We observed a similar pattern of results in the LFP, as shown in Fig. 7*B*. A two-way ANOVA revealed significant effects for both refresh rate and black/white ($P < 0.001$), with black LFP responses dominating white responses. Activity reductions for white stimuli were most notable at 60 Hz (R_{120}: 24%, R_{90}: 23%, R_{60}: 79%). The mean background

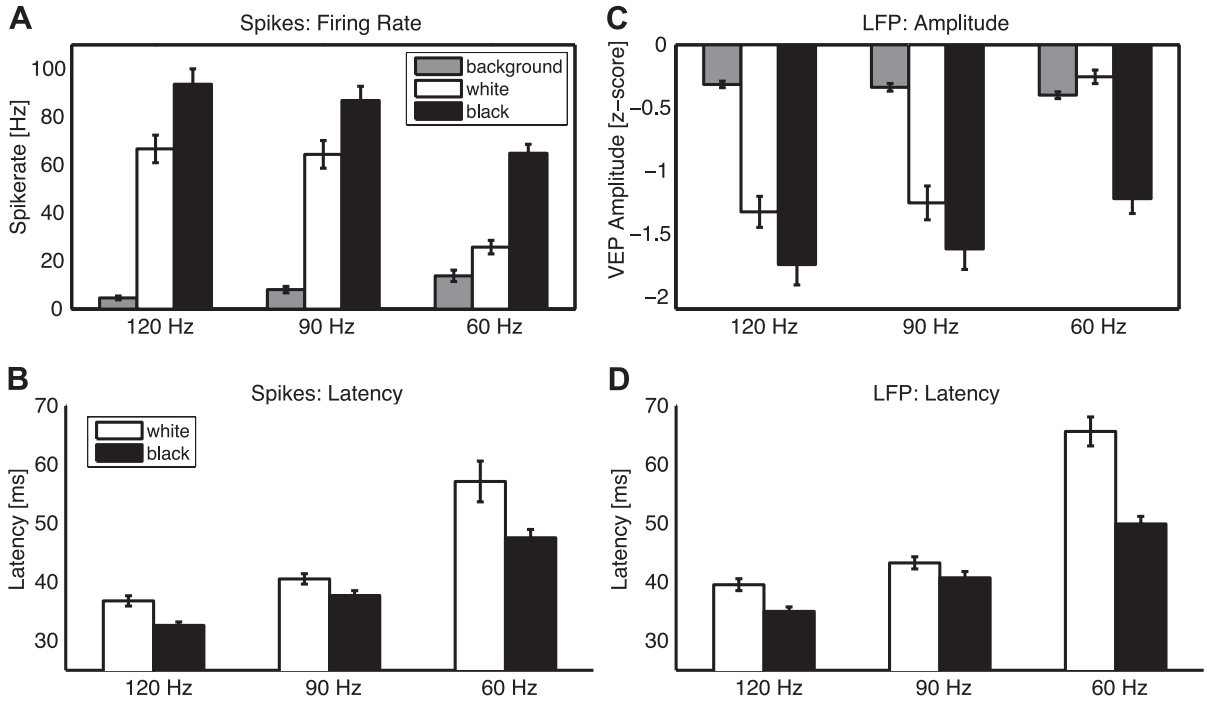

Fig. 7. Latency and amplitude of neural responses to white and black stimuli depend on refresh rate. *A*: average firing rate in a window from 25 to 110 ms after stimulus onset for the entire population of 52 units is shown for the three refresh rates separately for background (gray bars), white (white bars), and black (black bars) stimuli. Error bars: SE. *B*: same as *A* for the average LFP amplitude. *C*: population averaged response latencies of spiking activity shown for black and white stimuli separately at the three different refresh rates ($n = 51, 47, 48, 48, 25$, and 35 of 52 from *left* to *right*). Error bars: SE. *D*: same as *C* for LFP latencies ($n = 50, 51, 52, 52, 17$, and 50 of 52 from *left* to *right*).

Downloaded from jn.physiology.org on January 24, 2012

activity was similar for the different refresh rates (one-way ANOVA, $P = 0.1$).

Examining how cortical layer affected black dominance in spiking activity, we calculated a white-to-black ratio (WBR) for each unit (see MATERIALS AND METHODS) and compared its average value between supragranular ($n = 23$) and granular ($n = 19$) layers. We found significantly greater black dominance in supragranular layers than in granular layer IV (averages: $WBR_{120,supragranular}$, -0.53 ± 0.08; $WBR_{120,granular}$, -0.23 ± 0.06; $WBR_{90,supragranular}$, -0.53 ± 0.07; $WBR_{90,granular}$, -0.26 ± 0.05; $WBR_{60,supragranular}$, -1.61 ± 0.15; $WBR_{60,granular}$, -0.77 ± 0.08) consistently for all three monitor refresh rates (unpaired *t*-tests, $P < 0.01$).

In addition to eliciting stronger responses, black stimuli also activated V1 neurons earlier than white stimuli. To quantify this effect, we computed the response latency for each unit and LFP site (see MATERIALS AND METHODS). The resulting mean response latencies are shown in Fig. 7*C* for spiking activity (number of units with computable latency: $n_{120,white}$, 51; $n_{120,black}$, 47; $n_{90,white}$, 48; $n_{90,black}$, 48; $n_{60,white}$, 25; $n_{60,black}$, 45 of 52). Black responses had shorter latencies than white responses at all refresh rates. Importantly, response latencies were negatively correlated with refresh rate. At 60-Hz refresh rate, responses occurred around 15 ms later than at 120 Hz. A two-way ANOVA revealed the significance of both effects of black/white and refresh rate ($P \ll 0.001$). The LFP latency results, shown in Fig. 7*D*, followed exactly the same pattern (two-way ANOVA: effects of refresh rate and black/white, $P \ll 0.001$) (number of locations with computable latency: $n_{120,white}$, 50; $n_{120,black}$, 51; $n_{90,white}$, 52; $n_{90,black}$, 52; $n_{60,white}$, 17; $n_{60,black}$, 50 of 52). As for spiking, black stimuli evoked LFP responses faster than white stimuli, and LFP response latency was negatively correlated with refresh rate.

DISCUSSION

We have demonstrated that spiking responses in tree shrew V1 become entrained to the CRT monitor screen refresh. Entrainment was strongest at 60-Hz refresh rate and progressively declined with increasing refresh rate, although we still observed significant entrainment even at 120 Hz. Our results parallel observations in cats, monkeys and humans, which have reported entrainment of neural responses at refresh rates up to 100 Hz (Gur and Snodderly 1997; Krolak-Salmon et al. 2003; Lyskov et al. 1998; Williams et al. 2004; Wollman and Palmer 1995). The presence of entrainment in these diverse species suggests that it is probably inherited from a common ancestor, which must have lived at least 85 million years ago (Janecka et al. 2007; Liu et al. 2001; Murphy et al. 2001). Entrainment is a reflection of the high temporal precision of the visual system, which allows precise speed and distance judgments, and was probably conserved by evolution for these reasons. We extend the previously observed temporal precision results by showing that the LFP, like spiking activity, is also strongly locked to the monitor refresh. LFP locking was strongly correlated with locking of spiking activity at V1 sites. The LFP is a mass signal resulting from addition of electrical dipoles caused by synaptic inputs onto the dendrites of pyramidal cells. By contrast, spiking activity is related to action potential generation within V1 itself and thus reflects local computations in V1 neural circuits. Highly correlated and robust locking of both LFP and spiking signals is consistent with recent reports describing close correspondence of spiking and LFP in macaque V1 in terms of receptive field characteristics (Xing et al. 2009). The generally larger LRs of LFPs could be due to input from the visual thalamus, which has been shown to exhibit even stronger locking to visual transients than visual cortex (Wollman and Palmer 1995). We cannot, however, exclude methodological reasons for this quantitative difference because of the different nature of the two signals: continuous LFPs and binary spike trains.

Since these strongly entrained sensory afferent responses arrive in cortex in the granular layer IV, one might also expect stronger entrainment in this layer. This is exactly what we found, also in line with previous findings in macaque monkeys (Williams et al. 2004): entrainment was indeed weaker in supra- and infragranular layers, consistent with the idea that cortical processing tends to temporally broaden responses by inhibitory, horizontal, and feedback circuitry (Hawken et al. 1996; Oram 2010).

The high degree of entrainment even at 120 Hz suggests that the tree shrew visual system may be especially sensitive to high temporal frequencies, which would fit well with the lifestyle of this fast-moving, arboreal animal. Indeed, tree shrews are able to discern visual temporal modulation (luminance flicker) at frequencies up to ~70 Hz, with an optimal frequency of ~15 Hz (Callahan and Petry 2000). These values exceed those obtained in human subjects, where optimal frequency for luminance flicker detection is 10 Hz, and flicker becomes undetectable above ~40 Hz (Pantle 1971). In contrast to these psychophysical findings, neural signals in the human visual cortex encode temporal stimulus modulations at frequencies exceeding 70 Hz (Williams et al. 2004). Thus, consistently in both species, the frequency where temporal modulations can no longer be perceived is substantially lower than the frequency at which neural entrainment in V1 becomes undetectable. Similarly, visual cortex in both monkeys and humans responds to chromatic flicker at frequencies above ~25 Hz, but the two flickering colors are perceived as a monochromatic stimulus (Gur and Snodderly 1997; Jiang et al. 2007). Accordingly, visual stimulation at high temporal frequencies causes significant entrainment in cortical responses that appears to remain outside of conscious awareness. Note that, even though such fast changes remain imperceptible, they can still influence the perception of subsequently presented visual patterns (Falconbridge et al. 2010).

Taken together, the sensitivity for temporal visual stimulus modulations appears to be greater in tree shrew than in humans or macaque monkeys. Apart from this, however, there exist close parallels between tree shrew and primate species in terms of perception and neural entrainment to CRT-generated sequences of luminance transients like the contrast and layer dependence.

We found substantial differences in onset latency of visual responses as a function of monitor refresh rate: shortest onset latencies were observed for 120-Hz refresh rate, and reductions in refresh rate were associated with increases in onset latency. These effects were large in magnitude: at 60 Hz, onset latencies were ~15 ms greater than at 120 Hz, corresponding to an increase of ~30%. Previous work has demonstrated that stimulus attributes, such as size, contrast, and spatial frequency, have an impact on onset latencies in macaque and human

Downloaded from jn.physiology.org on January 24, 2012

visual cortex (Gawne et al. 1996; Mazer et al. 2002). We show that, maintaining identical visual stimulus attributes, variation of the refresh rate had a large impact on the onset latencies of V1 neural responses. To our knowledge, effects of stimulation frequency on onset latency have not been systematically investigated in monkeys or humans. However, we suggest that they may be related to psychophysical findings in human subjects: a recent study has described a 9-ms increase in reaction times to stimuli flickering at 70 Hz compared with identical stimuli flickering at 140 Hz (van Diepen et al. 2010). We suggest that slower arrival of neural activity in V1 at 70-Hz refresh rate, as evidenced by increased onset latencies, might be the reason for this behavioral slowing in reaction time. This emphasizes that refresh rate is an important parameter with large impact on neural response dynamics and probably also behavioral response times.

We observed that, on a gray background of intermediate luminance, light decrements (black stimuli) elicited faster responses than light increments (white stimuli). One possible reason for this could be that, technically, black stimuli could be considered to begin with the decay of the preceding luminance impulse, and thus almost one screen refresh earlier than white stimuli. We consider this unlikely, because black responses are also highly transient in nature and appear to be evoked by the local contrast generated by the continuous black stimulus embedded in the surrounding luminance impulses, corresponding to the gray background that is also present in the receptive field. The local contrast induced by the black stimulus thus occurs at exactly the same time as the white stimulus, suggesting that the observed latency differences are not artifacts of stimulus delivery.

In addition to these effects on latency, we have also demonstrated that black stimuli elicit larger responses than white stimuli, paralleling observations in macaque monkeys, where a similar dominance of black responses has been reported for both spiking and LFP (Xing et al. 2010; Yeh et al. 2009). These findings are thought to be related to the improved performance for black compared with white stimuli of human subjects in various psychophysical tasks (Bowen et al. 1989; Buchner and Baumgartner 2007; Krauskopf 1980; Short 1966; Whittle 1986). Interestingly, our results show that black/white differences are strongly dependent on refresh rate and cortical layer. V1 input layer activity is already biased toward stronger responses to black stimuli, and this difference is enhanced in the supragranular layers that mediate cortico-cortical communication. This enhancement is largely independent of refresh rate and approximately doubles the black preference. It is likely to be the result of a cortical mechanism (Xing et al. 2010; Yeh et al. 2009). The black stimulus bias in the input layer IV, however, is dependent on refresh rate and is about three times larger at 60 Hz than at 120 Hz. This input layer bias could result from local layer IV processing or be inherited from the retina or visual thalamus. The LFP results are consistent with these ideas: at 60 Hz, black dominance in the LFP is greatly enhanced, suggesting that the black dominance may already be present in the inputs to V1. In addition, weaker black preference in the LFP compared with spikes at higher refresh rates is expected for a local cortical mechanism, since LFPs are thought to largely reflect synaptic inputs (Rainer 2008).

A striking aspect of our results is the large difference in response attenuation we observed at the different refresh rates. At 120 Hz, both spiking and LFP responses were rapidly and strongly attenuated during visual stimulation with luminance impulses during a period of 80-ms duration. Each subsequent screen refresh evoked less activity than the preceding one, until, at the end of the 80-ms stimulation period, the response had declined by ~75%. This response attenuation may have an important functional role in contributing to adaptation, which dampens responses to static elements in the visual input, and assigns brain resources to moving or changing elements of the visual environment that are likely to have behavioral relevance (Kohn 2007; Tolias et al. 2005). At 120 Hz, the visual stimulus delivery elicits strong attenuation, as would be the case for real visual stimulation outside the laboratory, which is of continuous nature and not composed of luminance transients. By contrast, at 60-Hz refresh rate, we observed very little attenuation, and responses to subsequent luminance impulses were nearly independent. The different attenuation regimes at 60- and 120-Hz refresh rate might in fact explain why the "background response" was present at 60 Hz but not 120 Hz. At 120 Hz, neural activity has completely attenuated to the luminance impulses that make up the gray background, whereas at 60 Hz each luminance impulse is reflected in neural activity because there is very little attenuation. Our results have potential implications for functional magnetic resonance imaging (fMRI) studies, where adaptation is employed as a tool for probing cortical representations (Grill-Spector and Malach 2001). We suggest that the importance of monitor refresh rate on fMRI responses and their adaptation may have been severely underestimated and might have a substantial impact on observed fMRI responses in visual cortex. In particular, we suggest that, at least in V1, adaptation will play a minor role at 60 Hz and a prominent role at 120 Hz. Parametric variation of refresh rates could provide substantial new insights into visual representations in the human visual cortex. However, adaptation is only one possible candidate mechanism that might explain the nonlinear response attenuation we have observed. For example, conceptualizing this response attenuation as a nonlinear interaction between the flash and background responses might be a good alternative model to capture the observed dynamics in neural activity.

Taken together, we have demonstrated that CRT monitor refresh rate has a strong influence on neural response dynamics in tree shrew V1. Neural response parameters, such as onset latency, temporal profile, and temporal alignment of spikes, were all strongly affected by the refresh rate. Variation of these timing parameters due to factors such as stimulus type, contrast, or spatial frequency, have led to the idea that they might play an important role in neural coding (Optican and Richmond 1987; Oram et al. 2002; Reich et al. 2001; Richmond et al. 1987; Richmond and Optican 1987, 1990; Victor and Purpura 1996). The large variation in these parameters caused by changes in refresh rate for otherwise identical stimuli casts some doubt on the importance of the above neural response parameters for neural coding and representation of visual stimuli. Our findings rather suggest that visual representations may in fact be relatively invariant to changes in many aspects of temporal neural response dynamics. We have documented a number of close similarities between V1 of tree shrew and that of primates, such as macaque monkeys and humans. This

Downloaded from jn.physiology.org on January 24, 2012

suggests that mechanisms of information processing in tree shrew resemble those of primates in several important aspects concerning the temporal precision to visual stimulation, highlighting the usefulness of this small mammal for understanding visual function.

ACKNOWLEDGEMENTS

We thank D. Kerzel and E. Fuchs for helpful comments on the manuscript.

GRANTS

This work was supported by Swiss National Science Foundation ProDoc Grant PDFMP3_127179 and a European Young Investigator award to G. Rainer.

DISCLOSURES

No conflicts of interest, financial or otherwise, are declared by the author(s).

REFERENCES

Bosking WH, Crowley JC, Fitzpatrick D. Spatial coding of position and orientation in primary visual cortex. *Nat Neurosci* 5: 874–882, 2002.

Bowen RW, Pokorny J, Smith VC. Sawtooth contrast sensitivity: decrements have the edge. *Vision Res* 29: 1501–1509, 1989.

Buchner A, Baumgartner N. Text-background polarity affects performance irrespective of ambient illumination and colour contrast. *Ergonomics* 50: 1036–1063, 2007.

Callahan TL, Petry HM. Psychophysical measurement of temporal modulation sensitivity in the tree shrew (Tupaia belangeri). *Vision Res* 40: 455–458, 2000.

van Diepen RM, Born S, Souto D, Gauch A, Kerzel D. Visual flicker in the gamma-band range does not draw attention. *J Neurophysiol* 103: 1606–1613, 2010.

Falconbridge M, Ware A, MacLeod DIA. Imperceptibly rapid contrast modulations processed in cortex: evidence from psychophysics. *J Vis* 10: 21, 2010.

Gawne TJ, Kjaer TW, Richmond BJ. Latency: another potential code for feature binding in striate cortex. *J Neurophysiol* 76: 1356–1360, 1996.

Grieve KL, Acuña C, Cudeiro J. The primate pulvinar nuclei: vision and action. *Trends Neurosci* 23: 35–39, 2000.

Grill-Spector K, Malach R. fMR-adaptation: a tool for studying the functional properties of human cortical neurons. *Acta Psychol (Amst)* 107: 293–321, 2001.

Gur M, Snodderly DM. A dissociation between brain activity and perception: chromatically opponent cortical neurons signal chromatic flicker that is not perceived. *Vision Res* 37: 377–382, 1997.

Hawken MJ, Shapley RM, Grosof DH. Temporal-frequency selectivity in monkey visual cortex. *Vis Neurosci* 13: 477–492, 1996.

Van Hooser SD, Heimel JAF, Chung S, Nelson SB, Toth LJ. Orientation selectivity without orientation maps in visual cortex of a highly visual mammal. *J Neurosci* 25: 19–28, 2005.

Janecka JE, Miller W, Pringle TH, Wiens F, Zitzmann A, Helgen KM, Springer MS, Murphy WJ. Molecular and genomic data identify the closest living relative of primates. *Science* 318: 792–794, 2007.

Jiang Y, Zhou K, He S. Human visual cortex responds to invisible chromatic flicker. *Nat Neurosci* 10: 657–662, 2007.

Kohn A. Visual adaptation: physiology, mechanisms, and functional benefits. *J Neurophysiol* 97: 3155–3164, 2007.

Krauskopf J. Discrimination and detection of changes in luminance. *Vision Res* 20: 671–677, 1980.

Krolak-Salmon P, Hénaff MA, Tallon-Baudry C, Yvert B, Guénot M, Vighetto A, Mauguière F, Bertrand O. Human lateral geniculate nucleus and visual cortex respond to screen flicker. *Ann Neurol* 53: 73–80, 2003.

Liu FG, Miyamoto MM, Freire NP, Ong PQ, Tennant MR, Young TS, Gugel KF. Molecular and morphological supertrees for eutherian (placental) mammals. *Science* 291: 1786–1789, 2001.

Lyskov E, Ponomarev V, Sandström M, Mild KH, Medvedev S. Steady-state visual evoked potentials to computer monitor flicker. *Int J Psychophysiol* 28: 285–290, 1998.

Mazer JA, Vinje WE, McDermott J, Schiller PH, Gallant JL. Spatial frequency and orientation tuning dynamics in area V1. *Proc Natl Acad Sci U S A* 99: 1645–1650, 2002.

Murphy WJ, Eizirik E, O'Brien SJ, Madsen O, Scally M, Douady CJ, Teeling E, Ryder OA, Stanhope MJ, de Jong WW, Springer MS. Resolution of the early placental mammal radiation using Bayesian phylogenetics. *Science* 294: 2348–2351, 2001.

Optican LM, Richmond BJ. Temporal encoding of two-dimensional patterns by single units in primate inferior temporal cortex. III. Information theoretic analysis. *J Neurophysiol* 57: 162–178, 1987.

Oram MW, Xiao D, Dritschel B, Payne KR. The temporal resolution of neural codes: does response latency have a unique role? *Philos Trans R Soc Lond B Biol Sci* 357: 987–1001, 2002.

Oram MW. Contrast induced changes in response latency depend on stimulus specificity. *J Physiol (Paris)* 104: 167–175, 2010.

Pantle A. Flicker adaptation. I. Effect on visual sensitivity to temporal fluctuations of light intensity. *Vision Res* 11: 943–952, 1971.

Rainer G. Localizing cortical computations during visual selection. *Neuron* 57: 480–481, 2008.

Reich DS, Mechler F, Victor JD. Temporal coding of contrast in primary visual cortex: when, what, and why. *J Neurophysiol* 85: 1039–1050, 2001.

Richmond BJ, Optican LM, Podell M, Spitzer H. Temporal encoding of two-dimensional patterns by single units in primate inferior temporal cortex. I. Response characteristics. *J Neurophysiol* 57: 132–146, 1987.

Richmond BJ, Optican LM. Temporal encoding of two-dimensional patterns by single units in primate inferior temporal cortex. II. Quantification of response waveform. *J Neurophysiol* 57: 147–161, 1987.

Richmond BJ, Optican LM. Temporal encoding of two-dimensional patterns by single units in primate primary visual cortex. II. Information transmission. *J Neurophysiol* 64: 370–380, 1990.

Sesma MA, Casagrande VA, Kaas JH. Cortical connections of area 17 in tree shrews. *J Comp Neurol* 230: 337–351, 1984.

Shipp S. The brain circuitry of attention. *Trends Cogn Sci* 8: 223–230, 2004.

Short AD. Decremental and incremental visual thresholds. *J Physiol* 185: 646–654, 1966.

Tolias AS, Keliris GA, Smirnakis SM, Logothetis NK. Neurons in macaque area V4 acquire directional tuning after adaptation to motion stimuli. *Nat Neurosci* 8: 591–593, 2005.

Victor JD, Purpura KP. Nature and precision of temporal coding in visual cortex: a metric-space analysis. *J Neurophysiol* 76: 1310–1326, 1996.

Whittle P. Increments and decrements: luminance discrimination. *Vision Res* 26: 1677–1691, 1986.

Williams PE, Mechler F, Gordon J, Shapley R, Hawken MJ. Entrainment to video displays in primary visual cortex of macaque and humans. *J Neurosci* 24: 8278–8288, 2004.

Wollman DE, Palmer LA. Phase locking of neuronal responses to the vertical refresh of computer display monitors in cat lateral geniculate nucleus and striate cortex. *J Neurosci Methods* 60: 107–113, 1995.

Wong P, Kaas JH. Architectonic subdivisions of neocortex in the tree shrew (Tupaia belangeri). *Anat Rec (Hoboken)* 292: 994–1027, 2009.

Xing D, Yeh CI, Shapley RM. Spatial spread of the local field potential and its laminar variation in visual cortex. *J Neurosci* 29: 11540–11549, 2009.

Xing D, Yeh CI, Shapley RM. Generation of black-dominant responses in v1 cortex. *J Neurosci* 30: 13504–13512, 2010.

Yeh CI, Xing D, Shapley RM. "Black" responses dominate macaque primary visual cortex v1. *J Neurosci* 29: 11753–11760, 2009.

Downloaded from jn.physiology.org on January 24, 2012